



**Phase control in the colloidal synthesis of well-defined nickel sulfide nanocrystals**

Journal:	<i>Nanoscale</i>
Manuscript ID	NR-ART-06-2018-005208
Article Type:	Paper
Date Submitted by the Author:	28-Jun-2018
Complete List of Authors:	Barim, Gözde; University of Southern California, Chemistry Smock, Sara; University of Southern California, Chemistry Antunez, Priscilla; University of Southern California, Chemistry Glaser, Daniela; University of Southern California, Chemistry Brutchey, Richard; University of Southern California, Chemistry

# Phase control in the colloidal synthesis of well-defined nickel sulfide nanocrystals†

Gözde Barim, Sara R. Smock, Priscilla D. Antunez, Daniela Glaser and Richard L. Brutchey\*

*Department of Chemistry, University of Southern California, Los Angeles, CA 90089, USA*

E-mail: brutchey@usc.edu

Morphologically well-defined colloidal nanocrystals of  $\text{Ni}_3\text{S}_4$ ,  $\text{NiS}$ ,  $\text{Ni}_9\text{S}_8$ , and  $\text{Ni}_3\text{S}_2$  were independently prepared through a solution-phase synthesis using  $N,N'$ -disubstituted thioureas as the sulfur precursor. Synthetic control over phase and composition of the resulting colloidal nickel sulfide nanocrystals was achieved by primarily adjusting the reactivity of substituted thioureas as well as tuning the key reaction parameters of temperature and precursor ratio. In general, the more reactive  $N,N'$ -diphenyl thiourea yields more sulfur-rich phases ( $\text{Ni}_3\text{S}_4$  and  $\text{NiS}$ ) while less reactive  $N,N'$ -dibutyl thiourea yields sulfur-poor phases ( $\text{Ni}_9\text{S}_8$  and  $\text{Ni}_3\text{S}_2$ ). This phase control can be further tuned through the use of 1-dodecanethiol as an important secondary reactivity-directing agent. In the presence of 1-dodecanethiol, nanocrystals of more sulfur-deficient phases are prepared, while in the absence of 1-dodecanethiol, more sulfur-rich phases are prepared. Under the most sulfur-rich synthetic conditions (*i.e.*, with  $N,N'$ -diphenyl thiourea and no thiol) a phase progression from  $\text{Ni}_3\text{S}_4$  to the  $\alpha$ - $\text{NiS}$  and  $\beta$ - $\text{NiS}$  phases was observed upon an increase in reaction temperature and sulfur-to-nickel precursor ratio. This study establishes, for the first time, a systematic evaluation of factors that simultaneously control the phase and yield well-defined nickel sulfide nanocrystals.

## Introduction

Binary nickel sulfides exist in a complex phase space with a multitude of phases and compositions, including  $\text{NiS}_2$ ,  $\text{Ni}_3\text{S}_4$ ,  $\text{NiS}$ ,  $\text{Ni}_9\text{S}_8$ ,  $\text{Ni}_7\text{S}_6$ ,  $\text{Ni}_4\text{S}_3$  and  $\text{Ni}_3\text{S}_2$ . In 1962, Kullerud and Yund constructed a comprehensive binary Ni–S phase diagram for nickel sulfides.<sup>1</sup> According to their phase diagram,  $\text{Ni}_3\text{S}_2$  and  $\text{Ni}_3\text{S}_4$  are low-temperature phases, with rhombohedral  $\text{Ni}_3\text{S}_2$  (heazlewoodite) being the most nickel-rich phase. Above 843 K,  $\text{Ni}_3\text{S}_2$  transforms into a cubic polymorph.<sup>1</sup> Sulfur-rich  $\text{Ni}_3\text{S}_4$  (polydymite) possesses a cubic spinel structure that disproportionates into  $\text{NiS}$  and  $\text{NiS}_{1.03}$  above 373 K.<sup>2,3</sup> The  $\text{NiS}$  phase has two polymorphs —  $\beta$ - $\text{NiS}$  (millerite) is the low-temperature polymorph with a rhombohedral structure, and hexagonal  $\alpha$ - $\text{NiS}$  is the high-temperature polymorph. The  $\beta$ - $\text{NiS}$  to  $\alpha$ - $\text{NiS}$  phase transition takes place above 650 K in the bulk material, and the  $\alpha$ - $\text{NiS}$  phase has been shown to display a metal to insulator transition.<sup>4</sup> Distinct phases of these bulk nickel sulfides have been utilized as

electrocatalysts for hydrogen evolution reactions (HER)<sup>5–7</sup> and oxygen evolution reactions (OER)<sup>8–10</sup> for water splitting, electrode materials for lithium-ion<sup>11–13</sup> and sodium-ion batteries,<sup>14,15</sup> counter electrodes for dye-sensitized solar cells,<sup>16</sup> hydrodesulfurization catalysts,<sup>17</sup> and electroactive materials for supercapacitors.<sup>18</sup>

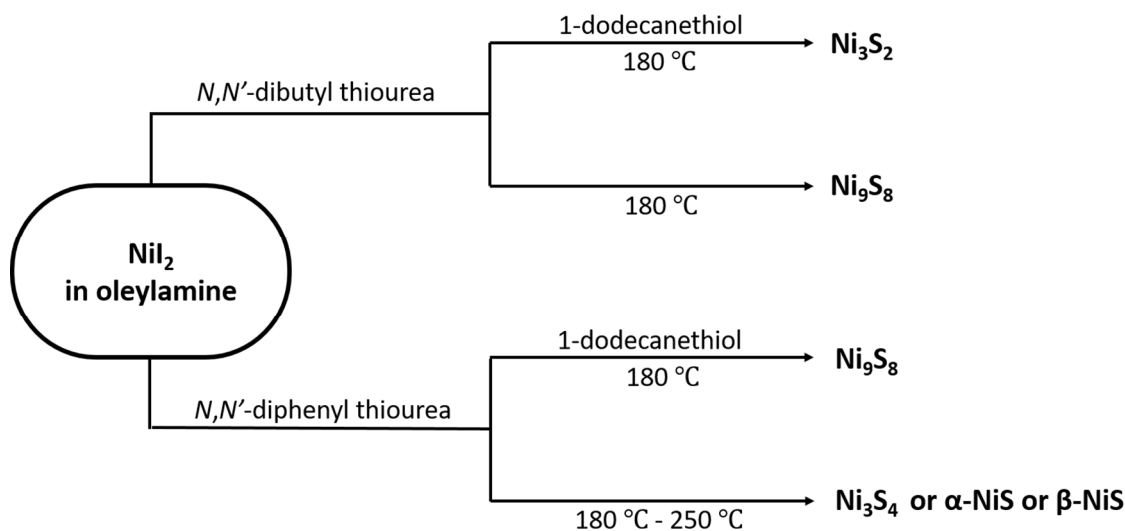
The preparation of colloidal nanocrystals with precise phase and morphology control is crucial because the functional properties of nanocrystals depend on the shape, size, crystal phase, and/or composition. However, the complicated nature of the Ni–S phase diagram makes the controlled solution-phase synthesis of colloidal nickel sulfide nanocrystals with simultaneously well-defined phase and morphology challenging.<sup>1,19,20</sup> There have been limited examples of the synthesis of well-defined colloidal nickel sulfide nanocrystals. For example, Korgel and coworkers reported the synthesis of nearly monodispersed and well-defined  $\beta$ -NiS nanorods and nanopyramids via thermal decomposition of nickel thiolate precursors in the presence of octanoic acid.<sup>21</sup> However,  $\text{Ni}_3\text{S}_4$  was found as an impurity phase in their as-synthesized  $\beta$ -NiS particles. More recently, Liu *et al.* demonstrated the shape-controlled synthesis of  $\text{Ni}_3\text{S}_4$  nanoparticles via a one-pot colloidal synthesis.<sup>22</sup> By varying the precursor concentration and using different nickel precursors, single-phase  $\text{Ni}_3\text{S}_4$  nanocrystals with two different, well-defined morphologies (*i.e.*, nanoprisms and nanopyramids) were prepared; however, this morphological control was only demonstrated for a single phase.

There have also been several recent examples of the phase-controlled synthesis of nanoscale nickel sulfides. Roffey *et al.* reported the preparation of colloidal nickel sulfides by using various nickel bis(dithiocarbamate) complexes as a single source precursor. By changing reaction conditions, such as temperature or precursor concentration, they were able to tune the phase of the resulting nickel sulfide nanoparticulates between  $\text{Ni}_3\text{S}_4$  and  $\alpha$ -NiS.<sup>23</sup> In a similar study, Gervas *et al.* demonstrated phase control over nickel sulfide nanoparticulates (*i.e.*,  $\text{Ni}_3\text{S}_4$  and  $\text{Ni}_3\text{S}_2$ ).<sup>24</sup> Pan *et al.* synthesized  $\text{Ni}_7\text{S}_6$ ,  $\alpha$ -NiS, and  $\beta$ -NiS nanoparticulates through the thermal decomposition of nickel acetylacetonate and 1-dodecanethiol in oleylamine or 1-octadecene. They observed that the Ni:S precursor ratio and solvent choice play a decisive role in the phase control of nickel sulfide nanostructures.<sup>25</sup> Although these three studies establish the influence of various reaction parameters on the control over nickel sulfide phase determination, they lack sufficient control over particle morphology, with the as-synthesized nanocrystals being polydispersed and possessing very ill-defined shapes. To the best of our knowledge, the ability to simultaneously exert control over phase and composition, and achieve well-defined morphologies, has yet to be broadly demonstrated for nanocrystals in the binary Ni–S system.

Herein, we report a parametric study on the phase-controlled synthesis of well-defined nickel sulfide nanocrystals using *N,N'*-disubstituted thioureas as the sulfur precursor and 1-dodecanethiol as a secondary reactivity-directing agent. By controlling precursor reactivity, a series of phase-pure nanocrystals of nickel sulfide with well-defined morphologies was achieved for the first time. Phase-pure nanocrystals of  $\text{Ni}_3\text{S}_4$ ,  $\alpha$ -NiS,  $\text{Ni}_9\text{S}_8$ , and  $\text{Ni}_3\text{S}_2$  with well-defined morphologies were independently prepared.

## Results and discussion

Nickel sulfide nanocrystals were synthesized via the fast addition of an *N,N'*-disubstituted thiourea into a hot solution of  $\text{NiI}_2$  in oleylamine. Substituted thioureas were chosen as the primary sulfur precursor because of their tunable conversion kinetics and ability to form monodispersed metal sulfide nanoparticles with a high degree of batch-to-batch consistency. Owen and co-workers previously demonstrated that the conversion rates of *N,N'*-disubstituted thioureas decrease upon the replacement of electron-withdrawing aryl groups with electron-donating alkyl substituents.<sup>26</sup> A less reactive *N,N'*-dibutyl thiourea was used in the synthesis of sulfur-deficient phases (*e.g.*,  $\text{Ni}_3\text{S}_2$ ). When 1-dodecanethiol was added 5 min after the injection of the primary sulfur precursor, the most sulfur-deficient  $\text{Ni}_3\text{S}_2$  phase was obtained. Sulfur-rich phases (*i.e.*,  $\text{Ni}_3\text{S}_4$ ,  $\alpha$ -NiS, and  $\beta$ -NiS) were synthesized in the absence of 1-dodecanthiol with the more reactive *N,N'*-diphenyl thiourea (Scheme 1).



**Scheme 1:** Reaction pathways using *N,N'*-disubstituted thioureas as the sulfur precursor, indicating the preparation of various nickel sulfide nanocrystal phases in the presence or absence of 1-dodecanethiol as the reactivity-directing agent.

### 1. Sulfur-Deficient Nickel Sulfide Phases

**Synthesis of  $\text{Ni}_3\text{S}_2$  nanocrystals.** An *N,N'*-dibutyl thiourea solution in dibenzylamine (10 molar equivalents relative to  $\text{NiI}_2$ ) was quickly injected into a solution of  $\text{NiI}_2$  in oleylamine at 180 °C, causing the greenish solution to turn black in *ca.* 3 min, indicating particle nucleation. After 5 min, 3.0 mL of 1-dodecanethiol was injected, and the reaction temperature was maintained at 180 °C for 1 h (Table S1). The powder X-ray diffraction (XRD) pattern of the resulting nanocrystals can be indexed to the rhombohedral heazlewoodite structure of the  $\text{Ni}_3\text{S}_2$  phase without any evidence of other crystalline Ni–S phases (Fig. 1a). The resulting nanocrystals possess a multipod morphology, as observed by transmission electron microscopy (TEM)

analysis (Fig. 1b,c). A high-resolution (HR-TEM) micrograph of a  $\text{Ni}_3\text{S}_2$  multipod arm suggests that the arms are single crystalline, with an interplanar distance of  $d = 4.0 \text{ \AA}$  that corresponds to the (101) planes of the rhombohedral heazlewoodite structure (Fig. 1d).

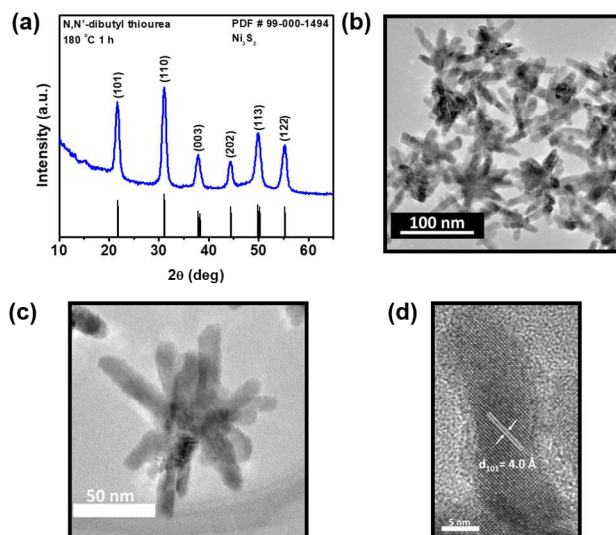


**Fig. 1** (a) XRD pattern of rhombohedral  $\text{Ni}_3\text{S}_2$  nanocrystals. (b) TEM micrograph of multipod-type  $\text{Ni}_3\text{S}_2$  nanocrystals. (c-d) HR-TEM micrographs of an individual  $\text{Ni}_3\text{S}_2$  nanocrystal.

It was found that 1-dodecanethiol used for this synthesis plays a decisive role in the formation of heazlewoodite  $\text{Ni}_3\text{S}_2$  nanocrystals. Under otherwise identical conditions, 10.0 molar equivalents of  $N,N'$ -dibutyl thiourea without the injection of 1-dodecanethiol gives nanocrystals of the relatively more sulfur-rich (but overall sulfur-poor) orthorhombic  $\text{Ni}_9\text{S}_8$  phase with rod-like aggregates (Fig. S1). The amount of thiol injected 5 min after  $N,N'$ -dibutyl thiourea also played a significant role in phase formation; that is, when the amount of 1-dodecanethiol was decreased to 0.3 mL, a mixture of  $\text{Ni}_3\text{S}_2$  nanocrystals along with some  $\text{Ni}_9\text{S}_8$  impurities were formed. When 1.5 mL of 1-dodecanethiol was injected, the resulting nanoparticles crystallize mainly into heazlewoodite  $\text{Ni}_3\text{S}_2$  phase, however, minor  $\text{Ni}_9\text{S}_8$  impurities were still found (Fig. S1a). These observations indicate that by varying the amount of 1-dodecanethiol, the nanocrystal phase can be tuned between  $\text{Ni}_3\text{S}_2$  and  $\text{Ni}_9\text{S}_8$ , and an increase in the amount of 1-dodecanethiol favors the more sulfur-poor rhombohedral  $\text{Ni}_3\text{S}_2$  phase over the orthorhombic  $\text{Ni}_9\text{S}_8$  phase. Formation of the more sulfur-deficient  $\text{Ni}_3\text{S}_2$  phase can be attributed to decreased conversion and growth kinetics of the nanocrystals in the presence of thiol (*vide infra*).

**Synthesis of  $\text{Ni}_9\text{S}_8$  nanocrystals.** Although phase-pure  $\text{Ni}_9\text{S}_8$  nanocrystals were obtained from the reaction of  $\text{NiI}_2$  and  $N,N'$ -dibutyl thiourea in the absence of 1-dodecanethiol, the resulting nanoparticles were ill-defined and aggregated (Fig. S1b). Hence, for the synthesis of more well-defined  $\text{Ni}_9\text{S}_8$  nanocrystals, the more reactive  $N,N'$ -diphenyl thiourea was used as the primary sulfur precursor instead of  $N,N'$ -dibutyl thiourea. In this case,  $\text{NiI}_2$  was reacted with 3.0 molar equivalents of  $N,N'$ -diphenyl thiourea in oleylamine at 180 °C for 4 h (Table S1). As in the case

of the  $\text{Ni}_3\text{S}_2$  nanocrystal synthesis, 1-dodecanethiol was also injected 5 min after the injection of substituted thiourea to adjust the growth kinetics of the nanocrystals (Scheme 1). Fig. 2 gives the XRD pattern and TEM images of the as-synthesized nanocrystals. TEM micrographs of the nanocrystals reveal that they are highly uniform, quasi-spherical particles with an average diameter of  $8.8 \pm 1.8$  nm. The histogram of nanoparticle size is given in Fig. 2d, indicating a monomodal particle size distribution. Powder XRD analysis confirms that the nanocrystals possess the orthorhombic godlevskite structure of  $\text{Ni}_9\text{S}_8$ , with no evidence of other crystalline Ni–S phases (Fig. 2a). The high-resolution TEM image given in Fig. 2c shows lattice fringes of a single  $\text{Ni}_9\text{S}_8$  nanocrystal that have an interplanar distance of  $3.9 \text{ \AA}$ , corresponding to the  $d$ -spacing of the (112) planes of the godlevskite structure. To best of our knowledge, these nanocrystals are the smallest that have been reported for the orthorhombic  $\text{Ni}_9\text{S}_8$  phase.

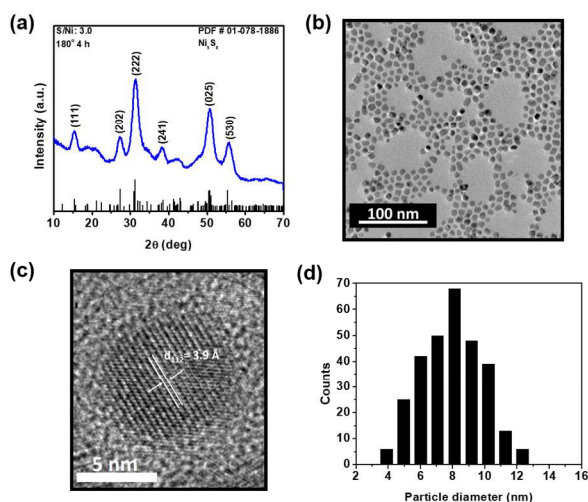


**Fig. 2** (a) XRD pattern of orthorhombic  $\text{Ni}_9\text{S}_8$  nanocrystals. (b) TEM micrograph of 8.8-nm  $\text{Ni}_9\text{S}_8$  nanocrystals. (c) HR-TEM micrograph of a single  $\text{Ni}_9\text{S}_8$  nanocrystal. (d) Size histogram showing the distribution of particle diameters for  $\text{Ni}_9\text{S}_8$  ( $N = 355$ ).

To elucidate the effect of 1-dodecanethiol on phase determination, several control reactions were performed in the presence and absence of thiol. Under otherwise identical conditions,  $N,N'$ -diphenyl thiourea was used as sole sulfur precursor, with no 1-dodecanethiol being injected subsequent to the injection of the thiourea solution. Fig. S2a compares the XRD patterns of the nickel sulfide nanocrystals synthesized in the presence and absence of 1-dodecanethiol under otherwise identical conditions. Powder XRD reveals that the nanocrystals comprise a mixture of relatively more sulfur-rich cubic  $\text{Ni}_3\text{S}_4$  and hexagonal  $\alpha$ -NiS phases in the absence of thiol. In contrast, the injection of either 1.5 or 3.0 mL of 1-dodecanethiol 5 min after the injection of  $N,N'$ -diphenyl thiourea gives phase-pure, sulfur-deficient, orthorhombic  $\text{Ni}_9\text{S}_8$  nanocrystals. The morphologies of the nanocrystals are comparable in the absence and presence of thiol, suggesting that the thiol has only a subtle impact on morphology (Fig. S2b). These results agree well with our previous observations about  $\text{Ni}_3\text{S}_2$  nanocrystal synthesis with  $N,N'$ -dibutyl thiourea in the presence of 1-dodecanethiol. In both cases, the injection of 1-dodecanethiol during the nanocrystal growth period have a substantial effect on phase determination. When 1-dodecanethiol is employed along with  $N,N'$ -disubstituted thioureas, it

acts as a reactivity-directing agent and favors the formation of more sulfur-deficient phases over the relatively more sulfur-rich phases (Scheme 1).

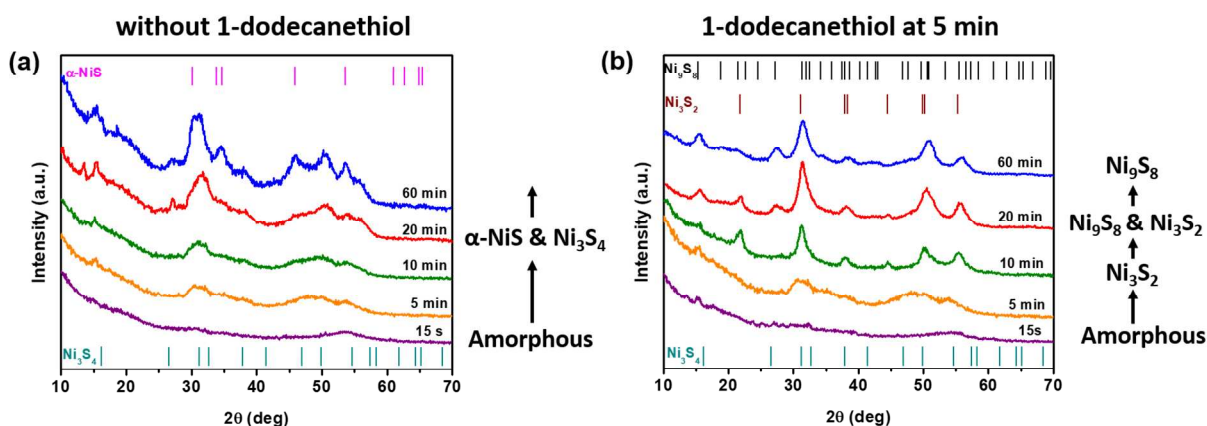


**Fig. 3** XRD patterns of the products from the reaction of  $\text{NiI}_2$  and 3.0 molar equivalents of  $N,N'$ -diphenyl thiourea at  $180^\circ\text{C}$  in the (a) absence and (b) presence of 1-dodecanethiol under otherwise identical conditions.

To gain insight into the phase evolution of these nanocrystals, aliquots were taken after 15 s, 5 min, 10 min, 20 min, and 60 min of reaction time in the absence and presence of 1-dodecanethiol, with  $t = 0$  indicating the injection of  $N,N'$ -diphenyl thiourea. Thiol was injected (if applicable) at  $t = 5$  min. Fig. 3 shows the phase evolution of the nickel sulfide nanocrystals under these conditions. In the absence of 1-dodecanethiol, the resulting product is completely amorphous after 15 s. After 5 min, broad diffraction peaks were observed that might be indexed to the cubic  $\text{Ni}_3\text{S}_4$  phase with hexagonal  $\alpha$ -NiS impurities that remained after 10 min. After 20 min, a mixture of the  $\text{Ni}_3\text{S}_4$  phase along with  $\alpha$ -NiS was still observed, and it remained as a mixed-phase product through at least 60 min (Fig. 3a). When an identical reaction was carried out in the presence of 1-dodecanethiol, a different phase evolution was observed after thiol addition. The first two aliquots taken at 15 s and 5 min give the same products to the reaction without thiol, resulting in largely amorphous products. Immediately after the second aliquot was taken at 5 min, 1.5 mL of 1-dodecanethiol was injected. In the presence of 1-dodecanethiol, the XRD pattern of the product from the aliquot taken at 10 min can be indexed to the rhombohedral  $\text{Ni}_3\text{S}_2$  phase, and at 20 min a mixture of  $\text{Ni}_3\text{S}_2$  and  $\text{Ni}_9\text{S}_8$  phases was observed (Fig. 3b). After 60 min, the product is completely converted into the orthorhombic  $\text{Ni}_9\text{S}_8$  phase, with no evidence of  $\text{Ni}_3\text{S}_2$  or any other crystalline Ni–S phases. This distinction in phase evolution of nanocrystals in the absence and presence of 1-dodecanethiol resembles the observations of Zhou *et al.* on  $\text{Cu}_2\text{ZnSnS}_4$  (CZTS) nanocrystals.<sup>27</sup> They reported phase control over CZTS nanocrystals by employing 1-dodecanethiol along with elemental sulfur and found that an increase in the amount of 1-dodecanethiol restrains the reactivity of sulfur leading to a phase evolution from kesterite phase to wurtzite phase. Our experiments clearly corroborate

that 1-dodecanethiol plays a decisive role in determining both the evolution and resulting phase of the nanocrystals, and favors the formation of sulfur-deficient  $\text{Ni}_9\text{S}_8$  and  $\text{Ni}_3\text{S}_2$  phases over sulfur-rich  $\text{Ni}_3\text{S}_4$  and  $\alpha\text{-NiS}$  phases.

$^1\text{H}$  NMR experiments were carried out to gain further insight into the effect of 1-dodecanethiol on the reactivity of  $N,N'$ -diphenyl thiourea. Identical reaction conditions for the synthesis of quasi-spherical  $\text{Ni}_9\text{S}_8$  nanocrystals were repeated in the absence of  $\text{NiI}_2$ . In other words,  $N,N'$ -diphenyl thiourea was dissolved in oleylamine, and the reaction mixture was heated to  $180^\circ\text{C}$ . The first aliquot was taken 10 min after reaching  $180^\circ\text{C}$ , and the second was taken 5 min after 1-dodecanethiol was injected into the reaction. Fig. S4 provides the  $^1\text{H}$  NMR spectra of aliquots and starting materials (*i.e.*,  $N,N'$ -diphenyl thiourea, oleylamine, and 1-dodecanethiol) in dichloromethane- $d_2$ . The  $^1\text{H}$  NMR spectra of  $N,N'$ -diphenyl thiourea dissolved in oleylamine shows the disappearance of the aromatic phenyl peaks at  $180^\circ\text{C}$  corresponding to the thiourea ( $\delta = 7.2\text{-}7.5$  ppm), indicating thermal decomposition of  $N,N'$ -diphenyl thiourea (Fig. S4b). Upon addition of 1-dodecanethiol, there are no apparent changes to the aromatic region of the  $^1\text{H}$  NMR spectrum, further confirming that the thermal decomposition of  $N,N'$ -diphenyl thiourea is independent of 1-dodecanethiol (Fig. S4b). This suggests that 1-dodecanethiol has no significant impact on the conversion kinetics of the  $N,N'$ -diphenyl thiourea since it is decomposed and nanocrystal nucleation is initiated before the injection of 1-dodecanethiol. Formation of sulfur-deficient nickel sulfide phases in the presence of 1-dodecanethiol can then be attributed to changes in the growth kinetics of the nanocrystals; that is, 1-dodecanethiol may form complexes with monomers that lead to slower diffusion and incorporation into growing nanocrystals, and/or it may bind to the nanocrystal surface and impede monomer incorporation resulting in the formation of more sulfur-deficient nanocrystals.<sup>28</sup>

In agreement with prior literature reports, we found that when 1-dodecanethiol is used as the sole sulfur precursor, it leads to the formation of orthorhombic  $\text{Ni}_9\text{S}_8$  nanocrystals with a rod-like morphology (Figs. S5 and S6, Table S2);<sup>11,29,30</sup> this morphology is dissimilar to the quasi-spherical particles achieved with  $N,N'$ -diphenyl thiourea and 1-dodecanethiol, and implies that when 1-dodecanethiol is added 5 min after the injection of thiourea, the 1-dodecanethiol is not acting as the primary sulfur source in the reaction, consistent with the fact that particle nucleation is observed prior to thiol addition.

## 2. Sulfur-Rich Nickel Sulfide Phases

**Effect of temperature and precursor ratio.** A series of reactions were carried out to gain insight into the influence of temperature and precursor ratio on the phase determination of the more sulfur-rich nickel sulfide nanocrystal phases with the more reactive  $N,N'$ -diphenyl thiourea as the sole sulfur precursor. First, the possibility of obtaining different nickel sulfide phases by changing the sulfur to nickel precursor ratio was investigated. By fixing the reaction time at 4 h and the temperature at  $180^\circ\text{C}$ , a series of reactions were performed with a range of S:Ni molar ratios between 3.0 and 6.0 in the absence of 1-dodecanethiol. The resulting powder XRD patterns indicate that the sulfur-rich cubic  $\text{Ni}_3\text{S}_4$  phase and hexagonal  $\alpha\text{-NiS}$  are present with a S:Ni precursor ratio of 3.0 (Fig. 4a). An increase in the intensities of the reflections at 30, 35,

and  $46^\circ 2\theta$  from  $\alpha$ -NiS was observed as the S:Ni precursor ratio increased to 4.0, with the intensities of the reflections from the  $\text{Ni}_3\text{S}_4$  phase concomitantly decreasing. With 5.0 molar equivalents of  $N,N'$ -diphenyl thiourea,  $\alpha$ -NiS is favored along with some minor impurity peaks from  $\text{Ni}_3\text{S}_4$ . In other words, the cubic  $\text{Ni}_3\text{S}_4$  phase appears to convert hexagonal  $\alpha$ -NiS phase by increasing the amount of sulfur precursor. At a S:Ni molar ratio of 6.0, the resulting nanocrystals exist mainly in the  $\alpha$ -NiS phase, along with minor amounts of  $\text{Ni}_3\text{S}_4$  and  $\beta$ -NiS impurities. This set of experiments demonstrates that the amount of  $N,N'$ -diphenyl thiourea plays a significant role in the phase determination of the nanocrystals, with an increase in the amount of sulfur precursor leading to the hexagonal  $\alpha$ -NiS and rhombohedral  $\beta$ -NiS phases being preferentially formed over cubic  $\text{Ni}_3\text{S}_4$  at  $180^\circ\text{C}$ . Simply considering a nickel sulfidation reaction, one would expect the formation of sulfur-rich  $\text{Ni}_3\text{S}_4$  nanocrystals at higher S:Ni ratios. Instead, our results resemble those of Korgel and Hayakawa, both of whom obtained the sulfur-rich  $\text{Ni}_3\text{S}_4$  phase at low sulfur precursor ratios.<sup>31,32</sup> Korgel *et al.* attributed this result to the faster sulfidation kinetics stemming from the small size of their nanocrystals.<sup>31</sup>

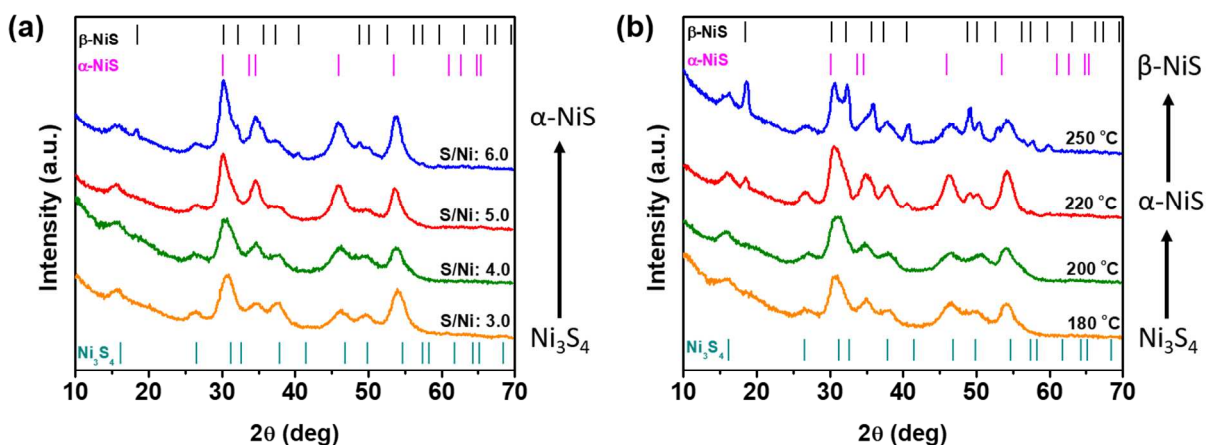


**Fig. 4** (a) Powder XRD patterns of the products from the reaction of  $\text{NiI}_2$  with  $N,N'$ -diphenyl thiourea as a function of S:Ni ratio; all reactions were carried out at  $180^\circ\text{C}$  for 4 h. (b) Powder XRD patterns of the products from the reaction of  $\text{NiI}_2$  with  $N,N'$ -diphenyl thiourea as a function of temperature for a 4 h reaction time with a fixed S:Ni molar ratio of 4.0.

Next, the role of the temperature on nanocrystal phase determination was explored by holding the S:Ni molar ratio and reaction time constant. A moderate S:Ni molar ratio of 4.0 was chosen and the reactions were carried out in a range of temperatures between  $180$  and  $250^\circ\text{C}$  for 4 h. The resulting XRD patterns indicate that the nanocrystals synthesized at  $180$  and  $200^\circ\text{C}$  crystallize into a mixture of the cubic  $\text{Ni}_3\text{S}_4$  and hexagonal  $\alpha$ -NiS phases (Fig. 4b). When the reaction temperature was increased to  $220^\circ\text{C}$ , the  $\alpha$ -NiS phase along with some impurities from  $\text{Ni}_3\text{S}_4$  and  $\beta$ -NiS were obtained. When the temperature was further increased to  $250^\circ\text{C}$ , the particles mainly crystallize into the rhombohedral  $\beta$ -NiS phase along with small amounts of  $\alpha$ -NiS and  $\text{Ni}_3\text{S}_4$  impurities. This set of experiments demonstrates that temperature also has a significant impact on phase determination; with increasing reaction temperature, a phase

preference from  $\text{Ni}_3\text{S}_4$  to  $\alpha\text{-NiS}$  and then  $\beta\text{-NiS}$  phase was observed. These results are in an agreement with previous reports, where  $\text{Ni}_3\text{S}_4$  has previously been shown to disproportionate at higher temperatures to give the  $\text{NiS}$  and  $\text{NiS}_{1.03}$  phases.<sup>33</sup> Based on these observations regarding the influence of precursor ratio and reaction temperature, we were able to design synthetic conditions for the preparation of phase-pure  $\text{Ni}_3\text{S}_4$  and  $\alpha\text{-NiS}$  nanocrystals.

**Synthesis of  $\text{Ni}_3\text{S}_4$  nanocrystals.** Polydymite  $\text{Ni}_3\text{S}_4$  is the major product of the reactions at low S:Ni precursor ratios and low temperatures (Fig. 4). Therefore, we reduced the S:Ni precursor ratio to 1.5 and characterized the product of the reaction between  $\text{NiI}_2$  and 1.5 molar equivalents of  $N,N'$ -diphenyl thiourea at 180 °C for 4 h (Table S1). XRD analysis reveals that the particles crystallize into the cubic polydymite structure of  $\text{Ni}_3\text{S}_4$ , with no evidence of  $\alpha\text{-NiS}$  or  $\beta\text{-NiS}$  impurities (Fig. 5a). The nanocrystals possess a mean diagonal length of  $12.4 \pm 2.4$  nm measured from  $\sim 300$  randomly chosen particles (Fig. 5d). An HR-TEM micrograph of an individual  $\text{Ni}_3\text{S}_4$  nanocrystal is given in Fig. 5c; the nanoparticle appears to be single crystalline with a lattice spacing of  $d = 5.5$  Å that matches well with the (111) plane of the cubic polydymite structure.

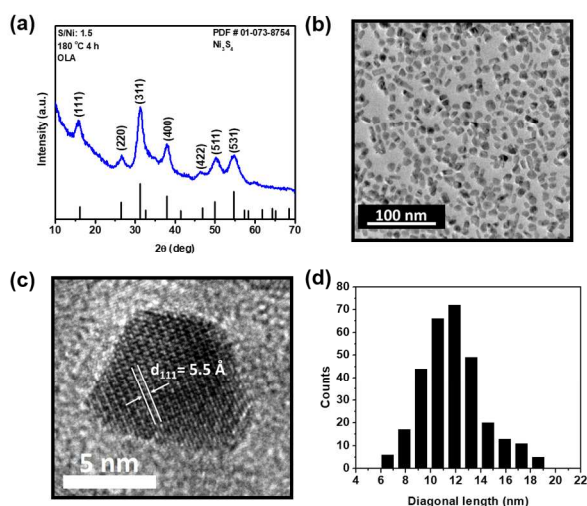


**Fig. 5** (a) XRD pattern of cubic  $\text{Ni}_3\text{S}_4$  nanocrystals. (b) TEM micrograph of 12.4-nm  $\text{Ni}_3\text{S}_4$  nanocrystals. (c) HR-TEM micrograph of an individual  $\text{Ni}_3\text{S}_4$  nanocrystal. (d) Size histogram showing the distribution of nanocrystal diameters for  $\text{Ni}_3\text{S}_4$  ( $N = 301$ ).

**Synthesis of  $\alpha\text{-NiS}$  nanocrystals.** The first set of experiments on the roles of precursor ratio and reaction temperature demonstrates that the  $\alpha\text{-NiS}$  phase is the major product of the reaction that was performed at 180 °C with a S:Ni molar ratio of 5.0 (Fig. 4). However, our attempts to obtain phase-pure  $\alpha\text{-NiS}$  nanocrystals by fine-tuning the temperature, precursor ratio and reaction time failed. Next, we employed different coordinating solvents/capping ligands other than oleylamine to prepare phase-pure  $\alpha\text{-NiS}$  nanocrystals, inspired by the previous studies showing phase control over nickel sulfide nanocrystals by varying the conversion kinetics of precursors with respect to the high-boiling solvents.<sup>24,30,34</sup> Recently, Revaprasadu *et al.*

reported phase control over colloidal nickel sulfide nanocrystals using single-source precursors in primary amine solvents.<sup>24</sup> In their study, dodecylamine, hexadecylamine, and oleylamine led to the formation of  $\text{Ni}_3\text{S}_4$ ,  $\text{Ni}_3\text{S}_2$ , and mixed phase particles, respectively, under otherwise identical conditions, which may be attributed to the difference in the precursor conversion kinetics of the single-source precursor as a function of amine solvent. Similarly, Owen *et al.* reported a difference in the conversion kinetics for *N*-phenyl-*N'*-dodecyl thiourea in different high-boiling solvents.<sup>26</sup>

In order to prepare phase-pure  $\alpha$ -NiS, we kept S:Ni ratio of 5.0 constant and used dodecylamine in place of oleylamine as the coordinating solvent. *N,N'*-diphenyl thiourea was quickly injected into the  $\text{NiI}_2$  solution at 180 °C, and the reaction was maintained at that temperature for 5 min (Table S1). Powder XRD analysis reveals that the product is composed of hexagonal  $\alpha$ -NiS with no evidence of any  $\text{Ni}_3\text{S}_4$  or  $\beta$ -NiS impurities (Fig. 6a). The resulting nanocrystals are quasi-spherical, with an average particle diameter of  $8.9 \pm 2.4$  nm determined by TEM analysis (Fig. 6b-d). An HR-TEM image of an individual nanocrystal is shown in Fig. 6c, which suggests that the particle is single-crystalline with a measured interplanar spacing of  $d = 2.5$  Å being in good agreement with the  $d$ -spacing of the (101) planes of hexagonal  $\alpha$ -NiS. According to bulk phase diagram of nickel sulfide, the  $\alpha$ -NiS phase is the high-temperature polymorph with the  $\beta$ -NiS phase being thermodynamically preferred;<sup>1,19</sup> however, on the nanoscale, a kinetically trapped metastable  $\alpha$ -NiS phase is being formed at lower temperatures.<sup>24</sup>

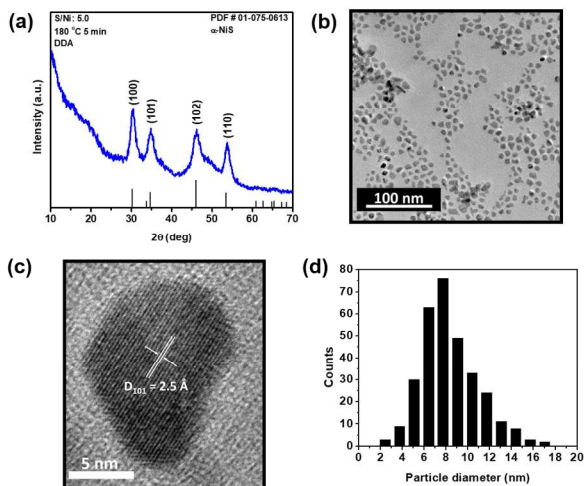


**Fig. 6** (a) XRD pattern of hexagonal  $\alpha$ -NiS nanocrystals. (b) TEM micrograph of 8.9-nm  $\alpha$ -NiS nanocrystals. (c) HR-TEM micrograph of an individual  $\alpha$ -NiS nanocrystal. (d) Size histogram showing the distribution of nanocrystal diameters for  $\alpha$ -NiS ( $N = 300$ ).

**Synthesis of  $\beta$ -NiS nanocrystals.** We further attempted to obtain phase-pure  $\beta$ -NiS nanocrystals. In the series of reactions as a function of S:Ni ratio and temperature,  $\beta$ -NiS impurities were observed at a S:Ni ratio of 6.0 and the reaction temperature of 180 °C.

Similarly, when the reaction temperature was increased to 220 °C, the  $\beta$ -NiS phase was observed to be the major product with a S:Ni ratio of 4.0 (Fig. 4). Therefore, we tried to fully convert  $\alpha$ -NiS nanocrystals to the thermodynamically favored  $\beta$ -NiS phase by the aid of increasing reaction temperature and S:Ni precursor ratio. The reaction of NiI<sub>2</sub> with an 8.0 molar excess of *N,N'*-diphenyl thiourea in oleylamine at 220 °C for 4 h gives a product primarily indexed to the millerite  $\beta$ -NiS phase with a rhombohedral structure by XRD (Table S1); however, some minor impurity peaks from hexagonal  $\alpha$ -NiS were still found (Fig. S7a).

## Conclusion

Slower conversion kinetics in the reaction with *N,N'*-dibutyl thiourea in the presence of 1-dodecanethiol result in the formation of the most sulfur-deficient Ni<sub>3</sub>S<sub>2</sub> phase, with the morphology of the final product being dictated by the amount of 1-dodecanethiol used in the synthesis. In contrast, the more sulfur-rich Ni<sub>3</sub>S<sub>4</sub> and NiS phases are obtained with the more reactive *N,N'*-diphenyl thiourea precursor in the absence of 1-dodecanethiol. The combination of 1-dodecanethiol with the more reactive *N,N'*-diphenyl thiourea appears to temper the growth kinetics of the nanocrystals and favor formation of the relatively less sulfur-rich Ni<sub>9</sub>S<sub>8</sub> phase. Tunable conversion kinetics of *N,N'*-disubstituted thioureas also affects particle morphology. Relatively bigger and more polydispersed nanocrystals are obtained when *N,N'*-dibutyl thiourea is used as the sole sulfur precursor, whereas faster conversion kinetics with *N,N'*-diphenyl thiourea result in smaller and nearly monodispersed quasi-spherical nanocrystals. These results are in a good agreement with previous studies. Owen *et al.* reported synthesis of phase-impure nickel sulfide nanocrystals from the reaction of Ni(stearate)<sub>2</sub> with three different thioureas (*i.e.*, *N,N'*-diphenyl thiourea, *N*-phenyl-*N'*-*n*-dodecyl thiourea, and *N*-*n*-hexyl-*N'*-*N'*-di-*n*-butyl thiourea). They found that as-synthesized nanocrystals become polydispersed and ill-defined as the reactivity of the substituted thioureas decreases.<sup>26</sup>

Both the reaction temperature and S:Ni precursor ratio were demonstrated as being key parameters for the phase determination of the more sulfur-rich Ni<sub>3</sub>S<sub>4</sub>,  $\alpha$ -NiS, and  $\beta$ -NiS phases when *N,N'*-diphenyl thiourea was used as the sole sulfur precursor in the absence of 1-dodecanethiol. At a S:Ni ratio of 1.5 and a reaction temperature of 180 °C, phase-pure Ni<sub>3</sub>S<sub>4</sub> nanocrystals were obtained by using oleylamine as the solvent and capping ligand. In order to obtain phase-pure  $\alpha$ -NiS nanocrystals, dodecylamine was used as coordinating solvent instead of oleylamine, and the S:Ni precursor ratio was increased to 5.0. A further increase in the S:Ni ratio and reaction temperature results in the transformation of  $\alpha$ -NiS phase into primarily the  $\beta$ -NiS phase, which is the thermodynamically preferred phase. By developing a synthetic methodology for the solution-phase synthesis of a series of well-defined nanocrystals within the binary Ni–S phase space, this work can be utilized to facilitate further studies of this significant class of nanocrystals, along with their phase-dependent properties and applications.

## Experimental

**General Considerations.** Nickel (II) iodide ( $\text{NiI}_2$ , Alfa Aesar, 99.5%), *N,N'*-diphenyl thiourea (Alfa Aesar, 98%), *N,N'*-dibutyl thiourea (Alfa Aesar, 98%), oleylamine (*cis*-9-octadecenylamine, Sigma Aldrich, 70%), dodecylamine (1-aminododecane, Sigma Aldrich, 98%), dibenzylamine (Alfa Aesar, 98%) and 1-dodecanethiol (Sigma Aldrich, 98%) were all purchased and used without further purification. Nanocrystal syntheses were conducted under  $\text{N}_2$  using Schleck techniques in the absence of water and oxygen.

**$\text{Ni}_3\text{S}_2$  Nanocrystal Synthesis.**  $\text{NiI}_2$  (0.19 mmol, 0.06 g) and degassed oleylamine (15.2 mmol, 5.0 mL) were added to a three-neck flask fitted with a reflux condenser and rubber septa. The solution was heated to 120 °C and degassed for 30 min under vacuum. *N,N'*-dibutyl thiourea (1.9 mmol, 0.36 g) was dissolved in dibenzylamine (15.6 mmol, 3.0 mL) and the solution was sparged by bubbling nitrogen through it for 15 min. The solution of  $\text{NiI}_2$  in oleylamine was heated to 180 °C and then the solution of *N,N'*-dibutyl thiourea was quickly injected into the flask under flowing  $\text{N}_2$ . After 5 min, 1-dodecanethiol (12.5 mmol, 3.0 mL) was also injected into the reaction mixture and the reaction was allowed to proceed for 1 h with stirring under flowing  $\text{N}_2$ . The reaction was quenched by placing it in a water bath and allowing it to cool to room temperature.

**$\text{Ni}_9\text{S}_8$  Nanocrystal Synthesis.** In a typical synthesis,  $\text{NiI}_2$  (0.38 mmol, 0.12 g) and degassed oleylamine (15.2 mmol, 5.0 mL) were added to a three-neck flask fitted with a reflux condenser and rubber septa. The solution was heated to 120 °C and degassed for 30 min under vacuum. *N,N'*-diphenyl thiourea (1.14 mmol, 0.26 g) was dissolved in dibenzylamine (10.4 mmol, 2.0 mL) and the solution was sparged by bubbling  $\text{N}_2$  through it for 15 min. The solution of  $\text{NiI}_2$  in oleylamine was heated to 180 °C under flowing  $\text{N}_2$  and then the *N,N'*-diphenyl thiourea solution in dibenzylamine was quickly injected into the reaction flask. After 5 min, 1-dodecanethiol (12.5 mmol, 3.0 mL) was subsequently injected into the reaction mixture and then the reaction was allowed to proceed at 180 °C for 4 h with stirring under flowing  $\text{N}_2$ . After 4 h, the reaction was quenched by placing it in a water bath and allowing it to cool to room temperature.

**$\text{Ni}_3\text{S}_4$  Nanocrystal Synthesis.**  $\text{NiI}_2$  (0.38 mmol, 0.12 g) and degassed oleylamine (15.2 mmol, 5.0 mL) were added to a three-neck flask fitted with a reflux condenser and rubber septa. The solution was heated to 120 °C and degassed for 30 min under vacuum. *N,N'*-diphenyl thiourea (0.57 mmol, 0.13 g) was dissolved in dibenzylamine (7.8 mmol, 1.5 mL) and the solution was sparged by bubbling  $\text{N}_2$  through it for 15 min. The solution of  $\text{NiI}_2$  in oleylamine was heated to 180 °C, and then the *N,N'*-diphenyl thiourea solution in dibenzylamine was quickly injected into the reaction flask and allowed to react for 4 h with stirring under flowing  $\text{N}_2$ . The reaction was quenched by placing it in a water bath and allowing it to cool to room temperature.

**$\alpha$ -NiS Nanocrystal Synthesis.**  $\text{NiI}_2$  (0.38 mmol, 0.12 g) and degassed dodecylamine (21.7 mmol, 5.0 mL) were added to a three-neck flask fitted with a reflux condenser and rubber septa. The solution was cycled between vacuum and  $\text{N}_2$  several times at room temperature. *N,N'*-diphenyl thiourea (1.9 mmol, 0.43 g) was dissolved in dibenzylamine (15.6 mmol, 3.0 mL) and the solution was sparged by bubbling  $\text{N}_2$  through it for 15 min. The solution of  $\text{NiI}_2$  in dodecylamine

was heated to 180°C, and then the *N,N'*-diphenyl thiourea solution was quickly injected into the reaction flask and allowed to react for 5 min with stirring under flowing N<sub>2</sub>. The reaction was quenched by placing it in a water bath and allowing it to cool to room temperature.

**Nanocrystal Purification.** Nanocrystals were purified by precipitation in 25 mL of ethanol followed by centrifugation at 6000 rpm for 10 min. The supernatant was discarded. The precipitated nanocrystals were redispersed in 20 mL of hexanes and centrifuged again at 6000 rpm for 3 min, causing the larger particulates to settle. The precipitate was discarded, and the nanocrystals suspended in hexanes were reprecipitated again by addition of 20 mL of ethanol. The precipitated nanocrystals were finally dispersed in either hexanes or toluene. All workup procedures were carried out in air.

**Instrumentation.** Powder X-ray diffraction (XRD) analyses were performed on Rigaku Ultima IV X-ray diffractometer operated at 44 mA and 40 kV using a Cu K $\alpha$  radiation source ( $\lambda = 1.5406 \text{ \AA}$ ). Diffraction patterns were collected in the  $2\theta$  range of 10° to 70°. The step size and collection time were 0.008° and 1 s per step, respectively. All patterns were recorded under ambient conditions. Phases were assigned by the powder diffraction files of (PDFs) of the International Center Diffraction Data (ICDD) using Jade 9.0 software.

Transmission electron microscopy (TEM) imaging was performed on a JEOL JEM-2100 microscope at an operating voltage of 200 kV, equipped with a Gatan Orius CCD camera. Samples for TEM studies were prepared by drop-casting a stable suspension of nanocrystals in toluene on a 200 mesh Cu grid coated with a lacey carbon film (Ted Pella, Inc.).

All NMR spectra were collected on a Varian 600 MHz VNMRS spectrometer with 16 scans and a relaxation delay of 2 s and a tip angle of 30° to ensure that the pulse sequence generously exceeded the T1 times of the starting materials. The data was analyzed using MestReNova version 12.0.0 software. Samples were prepared in dichloromethane-*d*<sub>2</sub>.

†Electronic Supplementary information (ESI) available. See DOI:

## Conflicts of interest

There are no conflicts to declare.

## Acknowledgements

G.B. and R.L.B. acknowledge funding through the Department of Energy Office of Basic Energy Sciences under Grant No. DE-FG02-11ER46826.

## References

- (1) G. Kullerud and R. A. Yund, *J. Petrol.*, 1962, **3**, 126-175.
- (2) A. Manthiram and Y. U. Jeong, *J. Solid State Chem.*, 1999, **147**, 679–681.
- (3) A. Olivas, V. Petranovskii, M. Avalos, S. Fuentes and A. Olivas, *J. Vac. Sci. Tech. A.*, 1998, **16**, 3515–3520.
- (4) J. T. Sparks and T. Komoto, *Phys. Lett. A*, 1967, **25**, 398–399.
- (5) P. Luo, H. Zhang, L. Liu, Y. Zhang, J. Deng, C. Xu, N. Hu and Y. Wang, *ACS Appl. Mater. Interfaces*, 2016, **9**, 2500–2508.
- (6) Z. Qin, Y. Chen, Z. Huang, J. Su, Z. Diao and L. Guo, *J. Phys. Chem. C*, 2016, **120**, 14581–14589.
- (7) N. Jiang, Q. Tang, M. Sheng, B. You, D. Jiang and Y. Sun, *Catal. Sci. Technol.*, 2016, **6**, 1077–1084.
- (8) W. Zhou, X.-J. Wu, X. Cao, X. Huang, C. Tan, J. Tian, H. Liu, J. Wang and H. Zhang, *Energy Environ. Sci.*, 2013, **6**, 2921–2924.
- (9) H. Li, Y. Shao, Y. Su, Y. Gao and X. Wang, *Chem. Mater.*, 2016, **6**, 1077–1084.
- (10) L. Feng, G. Yu, Y. Wu, G. Li, H. Li, Y. Sun, T. Asefa, W. Chen and X. Zou, *J. Am. Chem. Soc.* 2015, **137**, 14023–14026.
- (11) K. Aso, H. Kitaura and A. Hayashi, *J. Mater. Chem.*, 2011, **21**, 2987–2990.
- (12) N. Mahmood and C. Zhang, Y. Hou, *Small*, 2013, **9**, 1321–1328.
- (13) A. A. AbdelHamid, X. Yang, J. Yang, X. Chen and J. Y. Ying, *Nano Energy*, 2016, **26**, 425–437.
- (14) D. Zhang, W. Sun, Y. Zhang, Y. Dou, Y. Jiang and S. X. Dou, *Adv. Funct. Mater.*, 2016, **26**, 7479–7485.
- (15) T. Wang, P. Hu, C. Zhang, H. Du, Z. Zhang, X. Wang, S. Chen, J. Xiong and G. Cui, *ACS Appl. Mater. Interfaces*, 2016, **8**, 7811–7817.
- (16) W. S. Chi, J. W. Han, S. Yang, D. K. Roh, H. Lee and J. H. Kim, *Chem. Commun.*, 2012, **48**, 9501–9503.
- (17) J. T. Klopogge, W. J. J. Welters, E. Booy, V. H. J. De Beer, R. A. Van Santen, J. W. Geus and J. B. H. Jansen, *Appl. Catal. A Gen.*, 1993, **9**, 77–85.
- (18) S.-W. Chou and J.-Y. Lin, *J. Electrochem. Soc.*, 2013, **160**, D178–D182.
- (19) R. Y. Lin, D. C. Hu and Y. A. Chang, *Metall. Trans. B*, 1978, **9**, 531–538.
- (20) R. C. Sharma and Y. A. Chang, *Metall. Trans. B*, 1980, **11**, 139–146.

- (21) A. Ghezelbash, M. B. Sigman and B. A. Korgel, *Nano Lett.*, 2004, **4**, 537–542.
- (22) L. Qingsheng, A. Diaz, A. Prosvirin, Z. Luo and J. D. Batteas, *Nanoscale*, 2014, **6**, 8935–8942.
- (23) A. Roffey, N. Hollingsworth, H. Islam, M. Mercy, G. Sankar, G. Hogarth and N. H. De Leeuw, *Nanoscale*, 2016, **8**, 11067–11075.
- (24) C. Gervas, S. Mlowe, M. P. Akerman, I. Ezekiel, T. Moyo and N. Revaprasadu, *Polyhedron*, 2017, **122**, 16–24.
- (25) Y. Pan, Y. Chen, X. Li, Y. Liu and C. Liu, *RSC Adv.*, 2015, **5**, 104740–104749.
- (26) M. P. Hendricks, M. P. Campos, G. T. Cleveland, I. Jen-La Plante and J. S. Owen, *Science* 2015, **348**, 1226–1230.
- (27) B. Zhou and Y. Wang, *RSC Adv.*, 2015, **5**, 70117–70126.
- (28) Y. Yin and A. P. Alivisatos, *Nature*, 2005, **437**, 664–670.
- (29) W.-Y. Wu, S. Chakraborty, C. K. L. Chan, A. Guchhait, M. Lin and Y. Chang, *Chem. Mater.*, 2014, **43**, 17445–17452.
- (30) K. Aso, A. Hayashi and M. Tatsumisago, *New J. Chem.*, 2014, **38**, 1731–1737.
- (31) A. Ghezelbash and B. A. Korgel, *Langmuir*, 2005, **21**, 9451–9456.
- (32) R. Karthikeyan, M. Navaneethan, J. Archana, D. Thangaraju, M. Arivanandhan and Y. Hayakawa, *Dalton Trans.*, 2014, **43**, 17445–17452.
- (33) Y. U. Jeong and A. Manthiram, *Inorg. Chem.*, **2001**, 78712, 73–77.
- (34) N. Hollingsworth, A. Roffey, H. Islam, M. Mercy, A. Roldan, A. Bras, W. Wolthers, M. Catlow, C. R. A. Sankar, G. Hogarth, and N. H. De Leeuw, *Chem Mater.*, 2014, **26**, 6218–6292.

## TOC

